Taylor & Francis
Taylor & Francis Group

FOCUS ISSUE ARTICLE

Mild selective photochemical oxidation of an organic sulfide using OxP-polyimide porous polymers as singlet oxygen generators

Jan Hynek[a]*, Daniel T. Payne[c]**, Lok Kumar Shrestha [a,d], Mandeep K. Chahal[a]***, Renzhi Ma[a], Jiang Dong[e], Katsuhiko Ariga [a,f], Yusuke Yamauchi[a,b,e] and Jonathan P. Hill[a]

[a]Research Center for Materials Nanoarchitectonics (MANA), National Institute for Materials Science (NIMS), Tsukuba, Japan;
[b]International Center for Young Scientists, National Institute for Materials Science (NIMS), Tsukuba, Japan;
[c]Department of Materials Science, Faculty of Pure and Applied Sciences, University of Tsukuba, Ibaraki, Japan;
[d]Department of Materials Process Engineering, Graduate School of Engineering, Nagoya University, Nagoya, Japan;
[e]Department of Advanced Materials Science, Graduate School of Frontier Sciences, The University of Tokyo, Kashiwa, Japan;
[f]Australian Institute for Bioengineering and Nanotechnology (AIBN), The University of Queensland, Brisbane, Australia

ABSTRACT

A series of porous organic polymers based on a singlet oxygen generating oxoporphyinogen ('**OxP**') has been successfully prepared from a pseudotetrahedral **OxP**-tetraamine precursor (**OxP(4-NH$_2$Bn)$_4$**) by its reaction with tetracarboxylic acid dianhydrides under suitable conditions. Of the compounds studied, those containing naphthalene (**OxP-N**) and perylene (**OxP-P**) spacers, respectively, have large surface areas (~530 m^2 g^{-1}). On the other hand, the derivative with a simple benzene spacer (**OxP-B**) exhibits the best ^{1}O$_2$ generating capability. Although the starting **OxP**-tetraamine precursor is a poor ^{1}O$_2$ generator, its incorporation into **OxP** POPs leads to a significant enhancement of ^{1}O$_2$ productivity, which is largely due to the transformation of NH$_2$ groups to electron-withdrawing diimides. Overall ^{1}O$_2$ production efficacy of **OxP-POP**s under irradiation by visible light is significantly improved over the common reference material **PCN-222**. All the materials **OxP-B**, **OxP-N** and **OxP-P** promote oxidation of thioanisole involving conversion of ambient triplet state oxygen to singlet oxygen under visible light irradiation and its reaction with the sulfide. Although the reaction rate of the oxidation promoted by **OxP** POPs is generally lower than for conventional materials (such as **PCN-222**) or previously studied **OxP** derivatives, undesired overoxidation of the substrate to methyl phenyl sulfone is suppressed. For organic sulfides, selectivity of oxidation is especially important for detoxification of mustard gas (bis(2-chloroethyl)sulfide) or similarly toxic compounds since controlled oxidation leads to the low toxicity bis(2-chloroethyl)sulfoxide while overoxidation leads to intoxification (since bis(2-chloroethyl)sulfone presents greater toxicity to humans than the sulfide substrate). Therefore, **OxP** POPs capable of promoting selective oxidation of sulfides to sulfoxides have excellent potential to be used as mild and selective detoxification agents.

CONTACT Lok Kumar Shrestha ✉ SHRESTHA.Lokkumar@nims.go.jp; Jonathan P. Hill ✉ Jonathan.HILL@nims.go.jp ▢ Research Center for Materials Nanoarchitectonics (MANA), National Institute for Materials Science (NIMS), Namiki 1-1, Tsukuba, Ibaraki 305-0044, Japan

*Institute of Inorganic Chemistry of the Czech Academy of Sciences, Husinec-Řež 1001, Řež 250 68, Czech Republic.
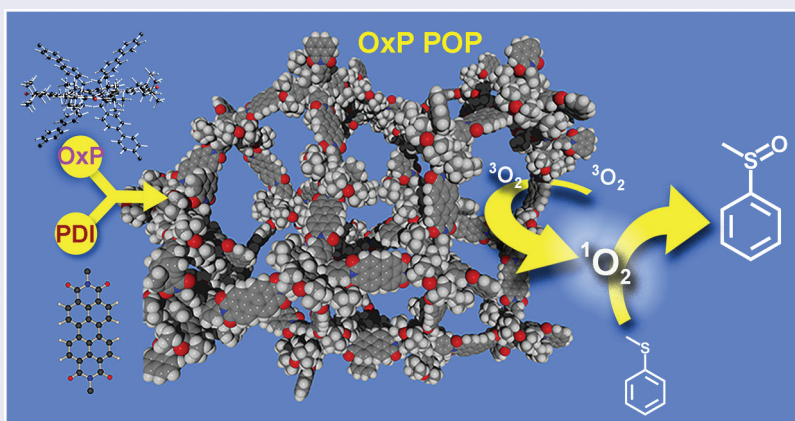**School of Life, Health and Chemical Sciences, The Open University, Walton Hall, Milton Keynes, MK7 6AA, United Kingdom.
***School of Chemistry and Forensic Science, University of Kent, Canterbury, CT2 7NH, United Kingdom.
▢ Supplemental data for this article can be accessed online at https://doi.org/10.1080/14686996.2024.2322458.

IMPACT STATEMENT
Oxoporphyrinogen (OxP) is a unique chromophore compound in that it is intrinsically de-aggregated allowing large quantum yields of singlet oxygen generation. Due to its structure, OxP is also an ideal building block for porous systems. In this work, we describe the first incorporation of OxP in highly stable microporous polymers strongly enhanced singlet oxygen generation for selective oxidation of organic sulfides to sulfoxides (as a model reaction) under heterogeneous conditions. The novelty of this work lies in the high stability and easy recovery of the materials, the synergetic enhancement of singlet oxygen generation in the polymers over the starting OxP, and the excellent selectivity for the oxidation reaction.

1. Introduction

Singlet oxygen ($^1O_2$) is a form of dioxygen generated by the excitation of ground (triplet) state O_2 molecules [1]. It is an important reactive oxygen species (ROS) with critical properties in biochemical systems [2,3] but it has also emerged as a very useful reagent for photodynamic therapy (PDT, of tumours [4,5], or for bacterial inactivation [6]), organic synthesis [7,8] or oxidation of chemical warfare agents [9,10]. For these reasons, novel means of generating singlet oxygen are continuously reported with applications involving photosensitization by an organic chromophore being highly attractive especially those based on white light or ambient light radiation, where a local power source is not required. While several chromophores have been proposed as $^1O_2$ photosensitizers including porphyrins [11], fullerenes [12] and conjugated polymers [13], these often suffer from deactivation processes, especially photobleaching [14]. These disadvantages can be partly or wholly overcome through incorporation of the chromophore into extended porous structures such as metal organic frameworks (MOFs) [15,16], covalent organic frameworks (COFs) [17] or porous organic polymers (POPs) [18], where chromophore bleaching is arrested but $^1O_2$ is able to emanate from the material at its surfaces or pores. These materials can be processed in film form or applied in microfluidic devices for the purposes of developing their potential applications [19]. The discovery of new chromophores suitable for these applications is therefore an intensively active area of research. Apart from MOFs and COFs several other classes of nanomaterials have been found to photocatalytically

generate $^1O_2$ and other reactive oxygen species (ROS) in a useful form. These catalysts include nitrogen-rich carbons [20], carbon nitride [21,22], and hexagonal boron nitride [23] all of which are capable of selective oxidation of sulfides for synthetic purposes or for environmental remediation.

Porous solids incorporating appropriate organic chromophores have been widely studied for ROS generation, especially for singlet oxygen ($^1O_2$) [24]. For example, Zr(IV)-MOF-based materials containing the 5,10,15,20-tetrakis(4-carboxyphenyl)porphyrin (TCPP) building block are widely studied with respect to their $^1O_2$ generation capabilities [25]. However, this property of MOFs is often limited by hydroxyl groups contained in the structure, which lead to substantial quenching of $^1O_2$ [26]. To ameliorate this effect, the active $^1O_2$-generating chromophore ought to be incorporated into a simple polymer structure (such as a POP) [27]. Consequently, POPs possessing $^1O_2$ generating capabilities have been used for the aforementioned applications (PDT [28], bacterial inactivation [29] or detoxification [30]. The latter of these applications might involve photochemical oxidation of, for example, mustard gas (bis(2-chloroethyl)sulfide) to its non-toxic sulfoxide congener. This process is notable here since it requires $^1O_2$ to act as mild oxidant thus avoiding overoxidation of bis(2-chloroethyl)sulfide and it's non-toxic sulfoxide to the also toxic bis (2-chloroethyl)sulfone [31]. POPs are a class of porous solids that, in contrast to MOFs [32], do not contain metallic nodes being composed solely of organic building blocks. POPs also differ from the commonly studied COFs [33] since they are usually non-

crystalline amorphous solids. The properties of POPs are strongly dependent on the type of bonding that is used for the connection of building blocks. Common linkage types are imine [34], boroxine [35], boronate ester [36] or triazine [37], despite the hydrolytic instability of some of these compounds, and the harsh conditions required for preparation of triazine POPs. In contrast, the condensation of oligoamines with tetracarboxylic acid dianhydrides such as 1,4,5,8-naphthalenetetracarboxylic dianhydride leads to diimide-bonded POPs with improved chemical stability by using simple preparative conditions [38]. As for other classes of porous solids, POPs have great potential for applications including gas storage [39], heterogeneous catalysis [40], sorption [41] and degradation [42] of pollutants, fluorescence sensing of explosives [43], etc.

In this study, we report the preparation of a series of diimide-linked POPs based on the oxoporphyrinogen 'OxP' chromophore as one of the building blocks. OxP is a chromophore molecule derived from 5,10,15,20-tetrakis(3,5-di-*tert*-butyl-4-hydroxyphenyl)porphyrin (T(DtBHP)P) by proton-coupled 2-electron oxidation [44]. In contrast to the parent porphyrin T(DtBHP)P, OxP has a non-planar macrocycle geometry similar to a calix [4]pyrrole [45] with pyrrolic N-H groups available for interaction [46] or substitution [47]. OxP and its derivatives have been studied as prochiral probes for chiral molecules [48], colorimetric sensors of ions [49],

organocatalysts [50] and electron acceptors in photosynthetic model systems [51]. Recently, we have also demonstrated that derivatives of OxP are efficient generators of $^1O_2$ operating under visible light irradiation by virtue of the main absorption band of the compounds appearing in the visible range with λ_{max} around 500 nm [52]. The properties of diimide-linked-OxP materials depend strongly on the identity of the anhydride used as the connecting unit, as well as on the reaction conditions used for the polymerization. The materials were found to have excellent potential for $^1O_2$-mediated oxidation reactions as indicated by the enhanced selectivity (over the corresponding oxo-Zr(IV) MOFs) in the oxidation of thioanisole to methyl phenyl sulfoxide. Figure 1(a) shows the chemical structures of the OxP diimide POPs, and Figure 1(b) shows the X-ray crystal structure of pristine unsubstituted OxP [53] with a calix [4]pyrrole-like conformation of the tetrapyrrole macrocycle. Figure 1(c) illustrates the tetrahedral conformation of the OxP POPs due to the disposition of pyrrole groups in the OxP-B compound prepared from OxP derivative OxP(4-NH$_2$Bn)$_4$ and pyromellitic anhydride, while Figure 1(d) is a space-filling representation of OxP-N, which indicates the possible steric role of the bulky macrocyclic *meso*-substituents in establishing a rigid building unit of any prospective polymeric structures. Figure 1(e) shows the structure of typical OxP-oxo-Zr (IV) MOFs (OxP-ZrMOF), which were initially studied for their $^1O_2$ generating capability [52].
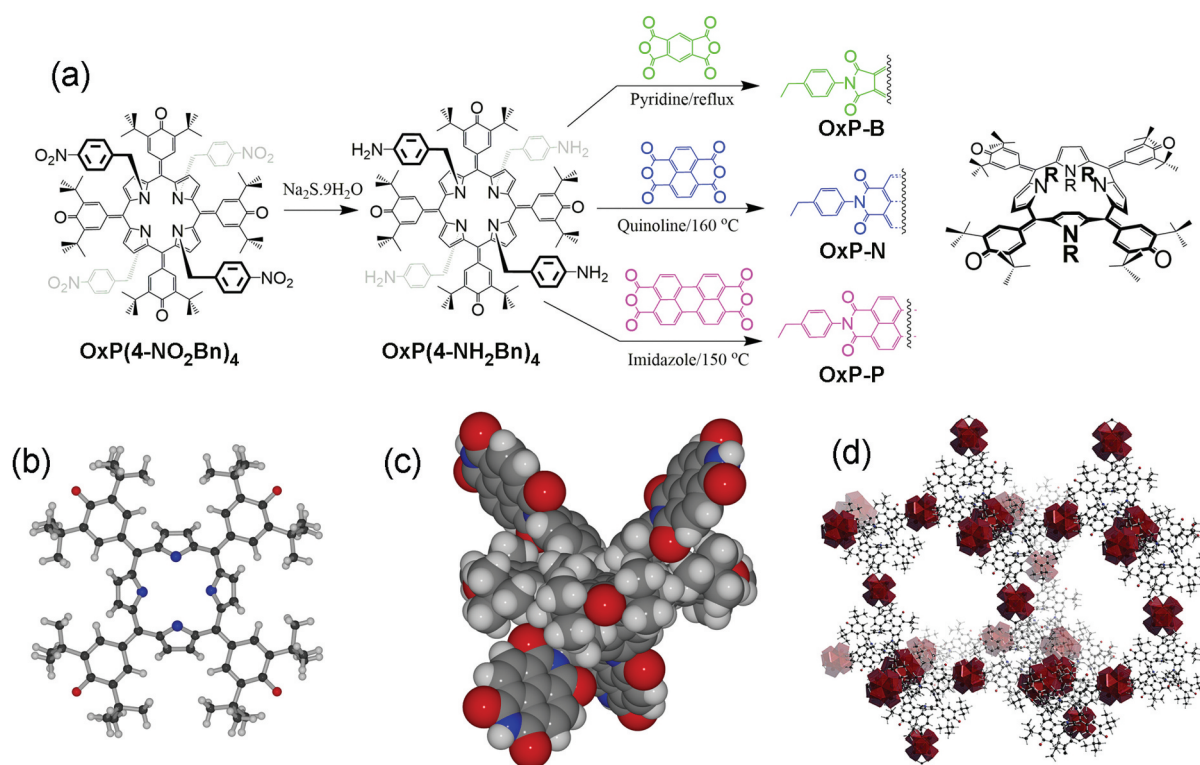

Figure 1. Synthesis and structures of OxP polyimide polymer singlet oxygen generators. (a) Synthesis and chemical structures of OxP POPs. (b) X-ray crystal structure of OxP [53]. (c) Space-filling representation of the energy-minimized (MM2) structure of the substituted OxP unit in OxP-B. Note the approximately tetrahedral disposition of its N-substituents [47]. (d) Diamondoid porous structure of OxP-ZrMOF previously studied for its singlet oxygen generation properties [52]. Panel (d) reproduced by permission from [52], copyright [2021, Elsevier Ltd].

2. Results and discussion

2.1. Structure and textural properties

OxP POPs were prepared from the **OxP(4-NH₂Bn)₄** building block, which was in turn prepared from the **OxP(4-NO₂Bn)₄** precursor (Figure 1). Although the reduction of 4-nitrobenzyl-substituted **OxP**s to the corresponding amine is convenient for lower multiplicities of N-substituent [54], the reduction of **OxP(NO₂Bn)₄** is accompanied by a significant amount of de-N-benzylation (mostly yielding the tri-N-benzyl-**OxP** derivative **OxP(4-NH₂Bn)₃** with one pyrrolic group de-alkylated, which was discarded). Reaction of **OxP(4-NH₂Bn)₄** with the 3 different aromatic tetracarboxylic dianhydrides yields the corresponding POPs designated according to the diimide spacer identity (**B** = **B**enzene tetracarboxylic acid diimide, **N** = **N**aphthalene tetracarboxylic acid diimide, **P** = **P**erylene tetracarboxylic acid diimide). Each material required a different method for its preparation after optimization. For pyromellitic dianhydride, reaction of **OxP(4-NH₂Bn)₄** in pyridine provided the solid polymeric product, while reaction with naphthalene-1,4,5,8-tetracarboxylic dianhydride was performed in quinoline at 160°C for 5 d. For perylene-3,4,9,10-tetracarboxylic dianhydride, the solid product was formed only when the reaction was performed in molten imidazole in the presence of Zn(OAc)₂ catalyst, probably due to the limited solubility of perylene-3,4,9,10-tetracarboxylic dianhydride.

The pXRD patterns of the **OxP** POPs (Figure S1) do not show any significant diffraction peaks due to the amorphous character of the materials, which is expected based on the synthesis of other diimide-linked polymers [55]. The presence of the diimide linkage of the polymers was confirmed by infrared spectroscopy of the materials (Figure S2) based on the red-shifted position (1710–1730 cm⁻¹) of the symmetrical C=O stretching absorptions, which usually appear around 1780 cm⁻¹ in aromatic anhydrides, and N – H stretching vibrations of the **OxP(4-NH₂Bn)₄** precursor (3200–3500 cm⁻¹) are completely eliminated suggesting complete conversion of – NH₂ group to diimide. The presence of two C=O (str.) peaks in **OxP-N** and **OxP-P** at 1730 and 1680 cm⁻¹ is similar to that for previously reported naphthalene diimides [56] and perylene diimides [57]. According to the particle size distributions of the materials obtained by DLS (Figure S3), **OxP-B** and **OxP-P** consist of large particles with diameters over 25 μm and a broad size distribution with particle diameters exceeding 1000 μm (the detection limit of the DLS instrument). In both samples, there are traces of smaller particles having diameters in the range 2–6 μm. For **OxP-N**, the particle size distribution is significantly narrower with particles mostly in the range 25–125 μm. Elemental compositions of the **OxP** POPs were measured using multiple independent methods. Combustion analysis (Table S1) shows that the contents especially of C and H are lower than expected calculated for polymers having infinite chains. This discrepancy is most likely due to excess oxygen present in the samples based on the presence of unreacted anhydride (or hydrolyzed dicarboxylic acid) groups at the surfaces of the materials. This was confirmed using EDX analysis (Figure S4) which revealed that the surfaces of the materials are composed largely of anhydride groups, since the observed C:O atomic ratio is in the range from 6.5:1 to 11.5:1; For comparison, the bulk material should exhibit C:O ratio in the range 10.5:1 to 13.5:1. For **OxP-P**, N content is almost double that expected and can be assigned to excess imidazole trapped in pores of the structure during synthesis (there are approximately 4–5 imidazole molecules incorporated per repeat unit of the polymer; this impurity could not be removed even after Soxhlet extraction over extended periods (>5 d). EDX analysis of **OxP-P** also indicates the presence of about 1 weight % of Zn originating from the zinc(II) acetate catalyst used during synthesis, which also persisted in samples even after extended extraction.

Textural properties of the **OxP** POPs were studied using N₂ sorption-desorption measurements. Analysis of the resulting adsorption isotherms (Figure 2(a)) provides the values of specific surface area (Table 1). The surface area of **OxP-B**, having the smallest linker between two neighbouring **OxP** moieties of the compounds studied, is around 130 m² g⁻¹ with the lower synthesis temperature probably leading to a lower extent of polymerization and low porosity. However, replacement of the benzene linker with naphthalene leads to a significant improvement in the surface area of **OxP-N** to 530 m² g⁻¹, which is similar to reported values of some other persistently porous polymers prepared by these methods [58]. The longer linker perylene does not lead to substantial increase in surface area although this could also be due to the irreversible incorporation of imidazole at the interior of **OxP-P**. The N₂ sorption-desorption isotherms show significant hysteresis due to difficult desorption of N₂ from the materials suggesting some elasticity of the structures. Also, pore size distributions of the materials calculated by the density functional theory (DFT) method (Figure 2(b)) confirm the presence of micropores in the 5–10 Å range and that these are most prevalent in **OxP-N**. For **OxP-B** and **OxP-P**, there is also a significant contribution by pore sizes in the 10–20 Å range.

During synthesis of the materials, we found that each of the **OxP** POPs requires a different method to establish the porous insoluble networks. This makes a direct comparison between the physical characteristics of the materials inconvenient since the differing synthesis procedures affect their pore sizes.
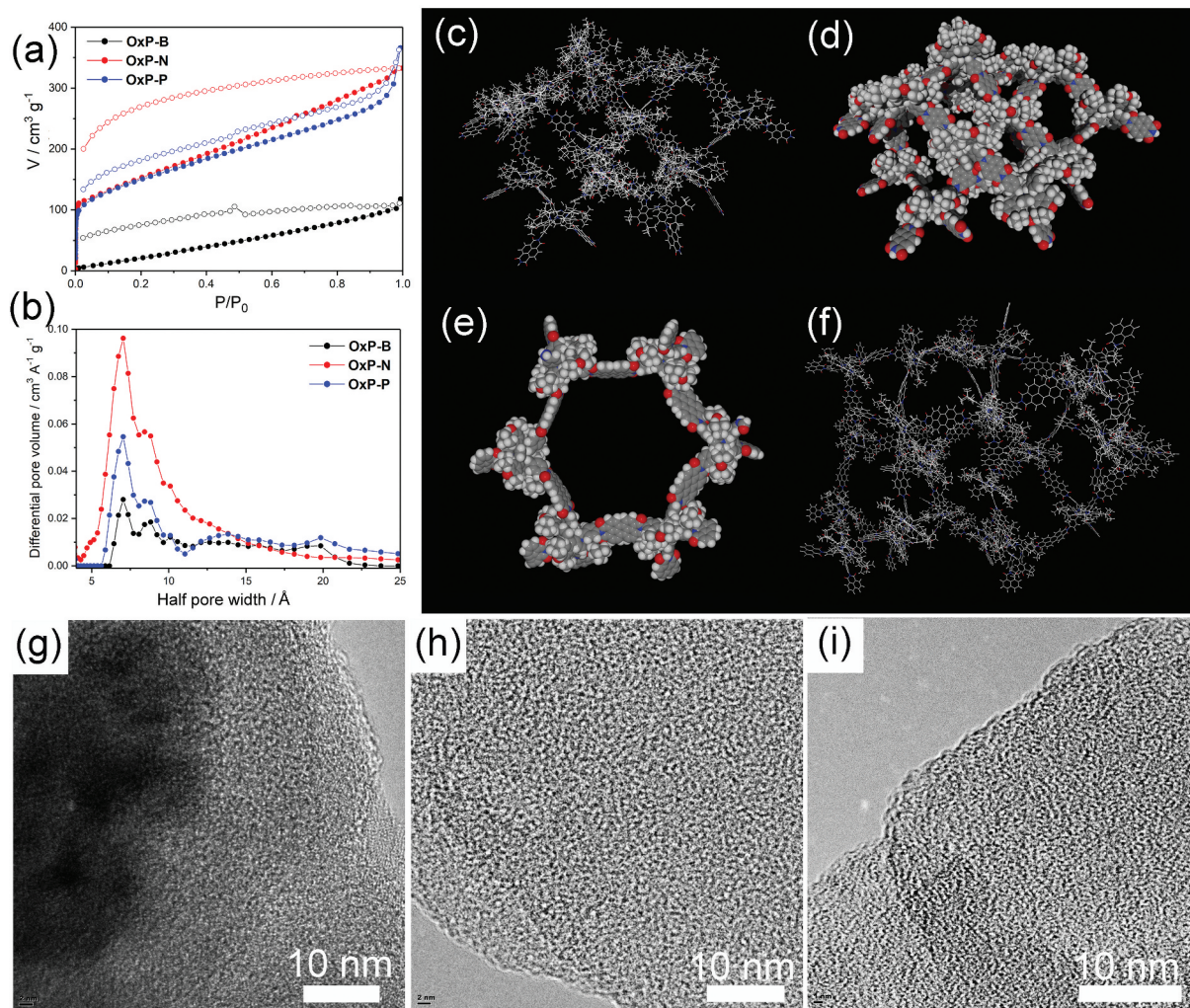
Figure 2. Textural parameters, simulated structures and TEM morphologies of **OxP** POPs. (a) N_2 adsorption isotherms of the **OxP** POPs measured at 77 K. (b) DFT pore size distributions calculated from the N_2 adsorption isotherms. Note that **OxP-N** has the largest proportion of pores in the 5–10 Å range while **OxP-P** and **OxP-B** have increasing proportions of larger pores in the 10–20 Å range. (c) Energy-minimized structure of a nanoparticle of **OxP-N** of approx. 10 nm diameter showing availability of pores based on rigid molecular components. (d) Space-filling representation of the **OxP-N** structure in (c). (e) Stable (energy-minimized) hexagonal pore structure (diameter 4 nm approx.) possible in **OxP-P** polymer. (f) Energy-minimized structure of a nanoparticle of **OxP-P** of approx. 10 nm diameter showing availability of pores based on rigid molecular components. TEM micrographs of (g) **OxP-B**, (h) **OxP-N**, and (i) **OxP-P** revealing amorphous microporous morphologies for the **OxP** POPs. See figure S5 for low resolution SEM and TEM images of the materials.

Table 1. Textural parameters of the **OxP** POPs studied.

Sample	S_{BET}/m^2 g^{-1}	V_{pore}/cm^3 g^{-1}
OxP-B	132	0.151
OxP-N	534	0.467
OxP-P	532	0.466

While it is difficult to make assertions about the effect of the pore size on the catalytic properties in this case, the aim of this work has simply been to obtain an optimum catalyst, which we have achieved based on variation of the inter-**OxP** linker. There is one observation that might be made based on the relative SO generating properties. While **OxP-B** shows qualitatively weaker singlet oxygen generating power than **OxP-N**, in acetonitrile **OxP-B** has enhanced oxidizing power of thioanisole over **OxP-N**. This might be as a result of the wider pore size

and greater accessibility of the substrate to the catalysts pores. In methanol, where reaction intermediates are stabilized, the two materials show similar activities possibly because access to pores is of lower priority in determining the reactivity.

Based on the lack of crystalline order in **OxP** POP materials and measurable porosity, we constructed model structures by randomly assembling the repeating units and performing energy minimization using the Materials Studio suite of programs. The resulting structures are shown in Figure 2(c-f). Figure 2(c) shows stick and space-filling representations of a particle (~10 nm) of **OxP-N** where large diameter pores are clearly persistent in the structure following the energy minimization procedure, which is consistent with the range of pore diameters extracted from Brunauer–Emmett–Teller (BET) isotherms. It is also

possible to construct regular pore geometries using these COF components (see Figure 2(e) for an energy minimized planar hexagonal pore in **OxP-P** having ~4 nm diameter) although pore size data suggests only a small population of these or similar pore architectures. The disordered structure of **OxP-P** obtained by energy-minimization using the Materials Studio program is shown in Figure 2(f) revealing a micropore architecture. The microporous structure of the materials is supported by transmission electron microscopy imaging shown in Figure 2(g–i). TEM images are typical of homogeneous microporous materials with larger mesopores visible at lower resolution (see Figure S5 for low resolution (SEM and TEM) electron microscopy images of the **OxP** POPs). The pore-structures of porous organic polymers can be rather disordered, so that observation of any ordered pore structure by electron microscopic

techniques is unlikely. Also, these **OxP** POP materials are solely organic also obstructing high-resolution TEM observation based on sample decomposition at higher voltages. TEM images, while of lower resolution do nevertheless indicate a disordered spongy porous forms of the materials as also indicated by their BET textural properties and powder diffraction patterns.

2.2. Photochemistry

Electronic absorption spectra of tetra-N-alkylated **OxP** derivatives contain a broad absorption band centered around 510 nm (Figure 3(a)), which extends from 400 to 650 nm. Rose Bengal, used as a reference here, absorbs at 550 nm (shoulder at 525 nm). Phosphorescence observed at 1270 nm due to $^1O_2$ formed in the presence of **OxP** POP precursor **OxP(4-NH$_2$Bn)$_4$** and Rose
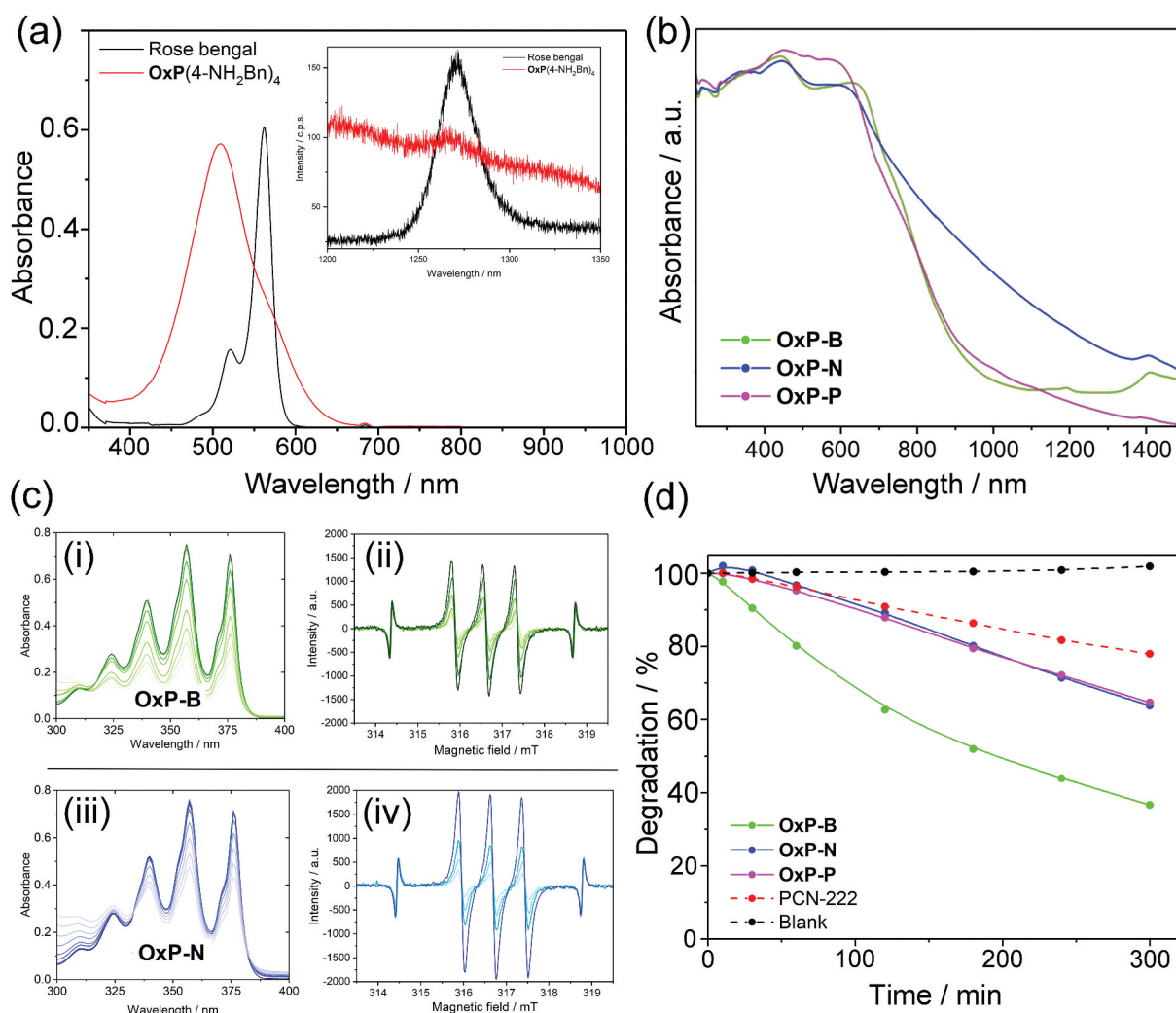

Figure 3. Electronic absorption spectroscopy. (a) UV-vis spectra of POP precursor **OxP(4-NH$_2$Bn)$_4$** and Rose Bengal (used as a reference $^1O_2$ generator in this study). Inset shows the phosphorescence emission peak due to $^1O_2$ generated by the respective dyes. Note the weak peak for **OxP(4-NH$_2$Bn)$_4$** (amines quench $^1O_2$) and the background emission tail due to **OxP** chromophore. (b) Solid state UV-vis spectra of **OxP** POPs. (c) Evidence for effective $^1O_2$ generation by **OxP-B** and **OxP-N**: (i) attenuation of anthracene electronic absorption by endoperoxide formation under irradiation (during 5 h) and (ii) ESR spectra measured in the presence of TEMP spin trap under irradiation in the presence of **OxP-B** POP (during 3 h) and (iii,iv) similar data (measured respectively over 5 h and 2 h periods) in the presence of **OxP-N** POP. (d) Decay in anthracene absorption in the presence of the **OxP** POPs, PCN-222 and without sensitizer (blank).

Bengal are shown in Figure 3a (inset) revealing that the precursor material is a poor $^1O_2$ generator ($\Phi_{SO} = 0.10$ vs. 0.76 for Rose Bengal). The absorption bands of **OxP** POPs (Figure 3(b)) are substantially broadened over the parent compound with a wide absorption covering most of the visible region of the electromagnetic spectrum from 300 to 800 nm. The broadening of the absorption band is due not only to inter-chromophore interactions at the materials' interiors but also to scattering caused by the particulate form of the samples. Increased and broadened absorbance and emission by **OxP** POPs obscures observation of the phosphorescence emission due to $^1O_2$ so that we have used other methods for its detection, namely, loss of anthracene UV-vis absorption by endoperoxide formation (Figure 3(c(i,iii))) and electron spin resonance spectroscopy (ESR) in the presence of the $^1O_2$-selective spin trap 2,2,6,6-tetramethyl-4-piperidinol (TEMP; Figure 3(c(ii,iv))). Data in Figure 3(c) clearly indicate the presence of $^1O_2$ (see Supplementary Information for related and control data). Figure 3(d) shows plots of anthracene UV-vis absorption attenuation accompanying endoperoxide formation based on $^1O_2$ generation by **OxP** POPs, reference PCN-222 and without sensitizer. Under these conditions, **OxP** POPs are clearly superior in activity over PCN-222, a commonly applied MOF-type $^1O_2$ generating material, with **OxP-B** eliminating up to 60% of anthracene after 5 h. While the data in Figure 3(c) and our other work [52,59] confirms the presence of $^1O_2$ generated by irradiation of the OxP chromophore in the presence of ambient dioxygen (e.g. TEMP spin trap is selective for $^1O_2$), there exists the possibility of the generation of other ROS such as hydroxyl radical or superoxide. However, for **OxP** chromophores such species have only been observed where protic processes (protonation and deprotonation) of the macrocycle are available [60,61]. For **OxPBn$_4$** type chromophores, which are difficult to protonate [62], processes leading to superoxide or hydroxyl radicals are absent, and only the excited triplet state of the irradiated chromophore can be involved in the photoexcitation of ground state dioxygen $^3O_2$.

As reported previously, tetra-N-alkylated **OxP** derivatives can serve as $^1O_2$ photosensitizers [52,59]. The precursor molecule of **OxP** POPs, **OxP(4-NH$_2$Bn)$_4$**, also generates $^1O_2$ under irradiation by 550 nm light, as indicated by the characteristic peak at 1270 nm in the photoluminescence spectrum (Figure 3(a)) [59]. The quantum yield of $^1O_2$ for **OxP(4-NH$_2$Bn)$_4$** in acetone is about 0.10, which is significantly lower than the **OxP** carboxylate esters studied previously ($\Phi_{SO} = 0.37$ for **OxP(4-(MeO$_2$C)Bn$_4$)** [52], due to the presence of amino groups which can quench any $^1O_2$ generated. For **OxP** POPs, few amino groups of the precursor remain (as indicated by FTIR spectra) so that this type of quenching is not expected. Additionally, it has recently been reported [59] that different tetra-N-alkylated **OxP**s are excellent $^1O_2$

generators especially when N-alkylating groups are relatively electron-withdrawing as is the case here for diimide N-substituents; quantum yields of $^1O_2$ generation approaching 0.90 were found for **OxP** derivatives [59]. Plots showing the attenuation of anthracene UV absorbance (Figure 3(b)) in irradiated solutions show that **OxP** POPs are superior to **PCN-222** in their $^1O_2$ generating capacities by a factor of ~ 2. A variety of factors might affect this including better harvesting of the light used for the irradiation (broad band visible light 400–700 nm) by the **OxP** chromophores over the porphyrin moiety in **PCN-222** and the morphologies of the samples, where larger irregular pores can increase the reaction interface with solution. **OxP** POPs have a comparable efficiency of $^1O_2$ production as the previously reported **OxP** porous coordination polymers (**OxP** PCPs) based on oxo-Zr(IV) clusters [52]. For **OxP** POPs, the absence of suppressing – OH groups in the structure should promote $^1O_2$ generation although the proximity of chromophores suggested by the broadness of the UV–vis absorption spectra implies relaxation of excited states by other routes with a negative effect on the $^1O_2$ productivity. Having confirmed formation of $^1O_2$ by irradiation of **OxP**-POPs according to in situ reaction with the spin trap (TEMP, see Figure 3(c) & S6 – S15) both in methanol and acetonitrile, these solvents were consequently used as the media for photooxidation studies. Relative $^1O_2$ generating efficacies of **OxP** POPs and **PCN-222** were estimated by in situ endoperoxidation of anthracene (see Figures S16 – S20).

2.3. Photooxidation of thioanisole

Since **OxP**-POPs produce $^1O_2$ at efficiencies comparable to or better than **PCN-222**, we decided to investigate their potential for the oxidization of organic substrates, in this case, thioanisole. Oxitation of thioethers can be used as a model reaction to assess the use of materials for the mild oxidation of toxic thioethers where oxidation of the substrate to a sulfoxide is preferred over its over oxidation to potentially toxic sulfones (e.g. mustard gas, bis (2-chloroethyl) sulfide; while mustard gas is a severe irritant its corresponding sulfoxide is almost inert but the corresponding sulfone is also a severe irritant [63]). Oxidation of thionanisole by $^1O_2$ as the oxidizing species ought to yield predominantly its sulfoxide (Figure 4(a)) although the respective sulfone (Figure 4(b)) might aso be formed. Selective oxidation of thioethers to sulfoxides can be considered based on their reaction with singlet oxygen. Initial reaction of the sulide with $^1O_2$ gives a reactive peroxide-like species $R_2S^+OO^-$, which is quenched by reaction with a further equivalent of the thioether yielding two equivalents of sulfoxide per equivalent of $^1O_2$ [64]. Other ROS such as peroxides have also been used for

this transformation but these often rely on a complicated catalyst system and overoxidation to the sulfone is a common disadvantage [65,66]. Hydroxyl radical can be used to oxidize sulfides but only in the presence of dioxygen, and the reaction mechanism proceeds by regenerating the starting sulfide so that high conversions attainable by using other methods are not usually acheivable [67].

Plots of the progress of reaction are also given in Figure 4(c-f) indicating that 1 mol% of **OxP-B** or **OxP-N** is sufficient to achieve nearly quantitative conversion to sulfoxide after 24 h in methanol (Figure 4(c,d)), respectively. In acetonitrile (Figure 4(e,f)) the activity

is significantly lower, although 80% conversion can be still be achieved with **OxP-B** in 24 h. We assume that the low activity of **OxP-P** is due to the incorporated imidazole molecules in the framework (imidazole is known to quench $^1O_2$ [68]).

As reference materials for comparison of the oxidation activity, we have used **PCN-222** and an **OxP-ZrMOF** previously reported by our group [52]. From Figure 4(c,f) it emerges that the activity of **OxP**-POPs is generally lower than **OxP-ZrMOF** but in some cases (**OxP-N** in methanol, **OxP-B** in both solvents) it is comparable to **PCN-222**. However, as can be seen from Figure 4(d,f) using **OxP** POPs is beneficial in
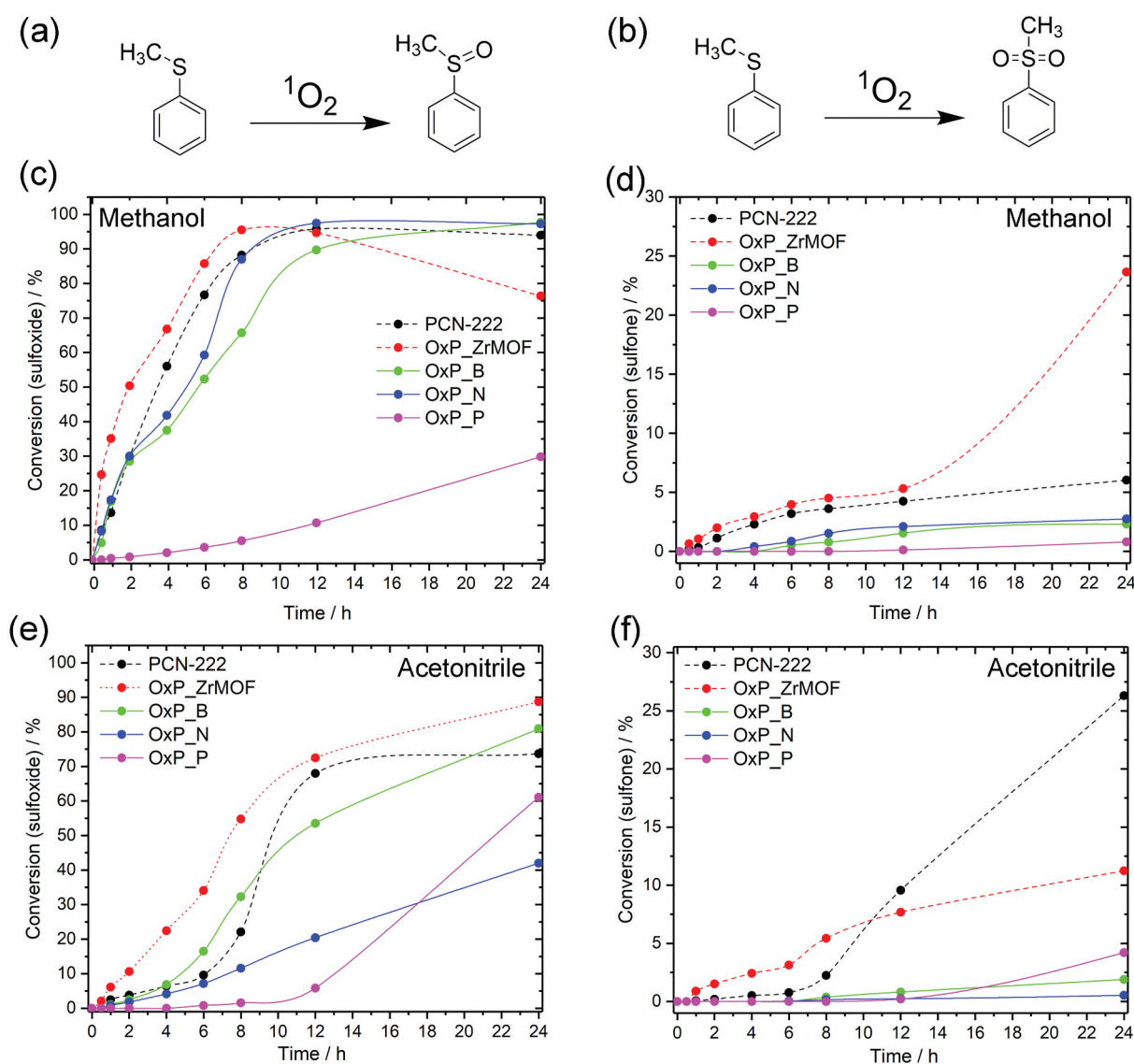

Figure 4. Conversion of thioanisole to its oxidation products by applying **OxP**-POP-generated $^1O_2$. (a) Oxidation of thioanisole to methyl phenyl sulfoxide. (b) Oxidation of thioanisole to methyl phenyl sulfone. (c) Percentage conversion to methyl phenyl sulfoxide for **OxP** POPs (1 mol% based on substrate) suspended with stirring in methanol-d_4 solutions of thioanisole ($c = 0.125$ M) irradiated with broad band visible light during 24 h. (d) Percentage conversion to methyl phenyl sulfone for **OxP** POPs (1 mol% based on substrate) suspended with stirring in methanol-d_4 solutions of thioanisole ($c = 0.125$ M) irradiated with broad band visible light during 24 h. (e) Percentage conversion to methyl phenyl sulfoxide for **OxP** POPs (1 mol% based on substrate) suspended with stirring in acetonitrile-d_3 solutions of thioanisole ($c = 0.125$ M) irradiated with broad band visible light during 24 h. (f) Percentage conversion to methyl phenyl sulfone for **OxP** POPs (1 mol% based on substrate) suspended with stirring in acetonitrile-d_3 methanol-d_4 solutions of thioanisole ($c = 0.125$ M) irradiated with broad band visible light during 24 h. Conversion was estimated using ^1H NMR spectroscopy after diluting (with CDCl$_3$) aliquots of the reaction mixture.

Table 2. Photocatalysts (**OxP-N**) stability for use in batch selective oxidation reactions.

Reaction run[a]	Conversion[b]/%	Yield (sulfoxide)
1	99.1	97.6
2	99.6	97.1
3	99.6	97.3
4	99.8	97.3
5	99.3	97.6

[a]For five consecutive 12 h reactions with photocatalyst recycling. [b]Based on integration of NMR peaks due to products (sulfoxide (2.74 ppm), sulfone (3.06 ppm)) and residual thioanisole (2.47 ppm).

terms of selectivity towards the sulfoxide product. As demonstrated by the appropriate NMR spectra (see Figure S21), 24 h of continuous irradiation of methanol dispersions of **OxP-ZrMOF** and **PCN-222** provided 24% and 6% of the overoxidized product, respectively, whereas in the case of **OxP-B** and **OxP-N** the concentration of methyl phenyl sulfone in the reaction mixture did not exceed ~ 2%, while full conversion to sulfoxide was achieved after 12 h of irradiation. Thus, **OxP-N** and **OxP-B** suspended in methanol can be considered as an excellent mild oxidation reagent system for the selective oxidation of sulfides to sulfoxides with the added benefit that the highly insoluble POP material can be simply removed by filtration following reaction completion further avoiding possible overoxidation scenarios. The filtered photocatalyst can be reused with virtually no loss of activity during multiple batch reaction runs over a more than 60 h period (see Table 2), which is an added advantage in the use of highly stable multichromophoric photocatalysts systems. The infrared spectrum of the photocatalyst remains essentially unchanged following its use during 60 h attesting to its excellent stability. Minor relative intensity changes found in the post-catalysis infrared spectrum can be assigned to small variations in solvation/hydration of the material. We note here that a similar **OxP** photocatalyst incorporated in a MOF structure [52] lost some activity in secondary batch reactions again emphasizing the excellent stability in use of the **OxP-N** photocatalyst. Finally, the catalysts remain active for several years when stored in the dark under ambient conditions attesting to their long-term stability.

3. Conclusion

A series of **OxP-POP**s has been successfully prepared from pseudotetrahedral $OxP(4\text{-}NH_2Bn)_4$ precursor by its reaction with carboxylic dianhydrides under suitable conditions. Of the compounds studied, **OxP-N** and **OxP-P** containing naphthalene and perylene spacers, respectively, have large surface areas (~530 $m^2\ g^{-1}$). On the other hand, **OxP-B** exhibits the highest $^1O_2$ generating capability. Although the starting $OxP(4\text{-}NH_2Bn)_4$ is a poor $^1O_2$ generator, incorporation of the compound into POPs leads to a significant enhancement of $^1O_2$ productivity, which is largely due to the transformation of NH_2 groups to electron-withdrawing diimides. The overall $^1O_2$ production efficacy of **OxP** POPs under irradiation by visible light is much improved over the common reference material **PCN-222**. All the materials **OxP-B**, **OxP-N** and **OxP-P** reveal significant activity to promote oxidation of thioanisole involving ambient oxygen under visible light irradiation. Although the reaction rate of the oxidation promoted by **OxP** POPs is generally lower than for conventional materials such as **PCN-222** or previously studied **OxP-ZrMOF**, analysis of the reaction mixtures reveals that undesired overoxidation of the substrate to methyl phenyl sulfone is suppressed. Therefore, **OxP**-POPs have excellent potential to be used as mild and selective oxidation agents for this purpose. Controllable oxidation is an important tool for instance in the selective transformation of benzyl alcohols to benzaldehydes [69], primary amines to imines [70], or organic sulfides to sulfoxides [71]. In the case of organic sulfides, selectivity of oxidation plays an especially important role in the detoxification of mustard gas (bis(2-chloroethyl)sulfide) or similar highly toxic compounds. Controlled oxidation provides the less harmful bis(2-chloroethyl)sulfoxide whereas overoxidation leads to intoxification since bis (2-chloroethyl)sulfone presents greater toxicity to humans than the sulfide substrate [72].

Disclosure statement

No potential conflict of interest was reported by the author(s).

ORCID

Lok Kumar Shrestha (ID) http://orcid.org/0000-0003-2680-6291

Katsuhiko Ariga (ID) http://orcid.org/0000-0002-2445-2955

References

[1] DeRosa MC, Crutchley RJ. Photosensitized singlet oxygen and its applications. Coord Chem Rev. 2002;233–234:351–371. doi: 10.1016/S0010-8545(02)00034-6

[2] Fujii J, Soma Y, Matsuda Y. Biological action of singlet molecular oxygen from the standpoint of cell signaling, injury and death. Molecules. 2023;28(10):4085. doi: 10.3390/molecules28104085

[3] Dogra V, Kim C. Singlet oxygen metabolism: from genesis to signaling. Front Plant Sci. 2022;10:1640. doi: 10.3389/fpls.2019.01640

[4] Hamblin MR. Photodynamic therapy for cancer: what's past is prologue. Photochem Photobiol. 2020;96(3):506–516. doi: 10.1111/php.13190

[5] Callaghan S, Senge MO. The good, the bad, and the ugly – controlling singlet oxygen through design of photosensitizers and delivery systems for photodynamic therapy. Photochem Photobiol Sci. 2018;17(11):1490–1514. doi: 10.1039/C8PP00008E

[6] Hamblin MR. Antimicrobial photodynamic inactivation: a bright new technique to kill resistant microbes. Curr Opin Microbiol. 2016;33:67–73. doi: 10.1016/j.mib.2016.06.008

[7] Nosaka Y, Nosaka A. Generation and detection of reactive oxygen species in photocatalysis. Chem Rev. 2017;117(17):11302–11336. doi: 10.1021/acs.chemrev.7b00161

[8] Pibiri I, Buscemi S, Piccionello AP, et al. Photochemically produced singlet oxygen: applications and perspectives. ChemPhotochem. 2018;2(7):535–547. doi: 10.1002/cptc.201800076

[9] Wagner GW, Yang YC. Rapid nucleophilic/oxidative decontamination of chemical warfare agents. Ind Eng Chem Res. 2002;41(8):1925–1928. doi: 10.1021/ie010732f

[10] Gephart RT, Coneski PN, Wynne JH. Decontamination of chemical-warfare agent simulants by polymer surfaces doped with the singlet oxygen generator zinc octaphenoxyphthalocyanine. ACS Appl Mater Interfaces. 2013;5(20):10191–10200. doi: 10.1021/am402897b

[11] Kou J, Dou D, Yang L. Porphyrin photosensitizers in photodynamic therapy and its applications. Oncotarget. 2017;8(46):81591–81603. doi: 10.18632/oncotarget.20189

[12] Hamblin MR. Fullerenes as photosensitizers in photodynamic therapy: pros and cons. Photochem Photobiol Sci. 2018;17(11):1515–1533. doi: 10.1039/C8PP00195B

[13] Blacha-Grzechnik A. New approach in the application of conjugated polymers: the light-activated source of versatile singlet oxygen molecule. Materials. 2021;14(5):1098. doi: 10.3390/ma14051098

[14] Tasso TT, Schlothauer JC, Junquiera HC, et al. Photobleaching efficiency parallels the enhancement of membrane damage for porphyrazine photosensitizers. J Am Chem Soc. 2019;141(39):15547–15556. doi: 10.1021/jacs.9b05991

[15] Song Y, Wang L, Xie Z. Metal-organic frameworks for photodynamic therapy: emerging synergistic cancer therapy. Biotechnol J. 2021;16:1900382. doi: 10.1002/biot.201900382

[16] Matlou GG, Abrahamse H. Nanoscale metal-organic frameworks as photosensitizers and nanocarriers in photodynamic therapy. Front Chem. 2022;10:971747. doi: 10.3389/fchem.2022.971747

[17] Alemán J, Mas-Ballesté R. Photocatalytic oxidation reactions mediated by covalent organic frameworks and related extended organic materials. Front Chem. 2021;9:708312. doi: 10.3389/fchem.2021.708312

[18] Zhang T, Xing G, Chen W, et al. Porous organic polymers: a promising platform for efficient photocatalysis. Mater Chem Front. 2020;4(2):332–353. doi: 10.1039/C9QM00633H

[19] Garcia-Fresnadillo DC. Singlet oxygen photosensitizing materials for point-of-use water disinfection with solar reactors. ChemPhotochem. 2018;2(7):512–534. doi: 10.1002/cptc.201800062

[20] Yang C, Ye H, Byun J, et al. N-rich carbon catalysts with economic feasibility for the selective oxidation of hydrogen sulfide to sulfur. Environ Sci Technol. 2020;54(19):12621–12630. doi: 10.1021/acs.est.0c02967

[21] Li S, Zhang Y, Li Y, et al. Modulating the photooxidation selectivity on graphitic carbon nitride by tuning edge functional groups. Appl Catal B - Environ. 2024;340:123180. doi: 10.1016/j.apcatb.2023.123180

[22] Lyu S, Wu W, Xiong R, et al. Carbon-rich carbon nitride nanocatalysts for H2S selective oxidation. J Catal. 2022;413:992–1004. doi: 10.1016/j.jcat.2022.08.011

[23] Yang H, Zeng L, Wang J, et al. Optimizing the electronic configuration of h-BN for bossting the photocatalytic transformation of acid gases under visible light. Environ Sci Adv. 2024;3:97–108. doi: 10.1039/d3va00239j

[24] Hynek J, Chahal MK, Payne DT, et al. Porous framework materials for singlet oxygen generation. Coord Chem Rev. 2020;425:213541. doi: 10.1016/j.ccr.2020.213541

[25] Feng D, Gu ZY, Li JR, et al. Zirconium-metalloporphyrin PCN-222: mesoporous metal–organic frameworks with ultrahigh stability as biomimetic catalysts. Angew Chem Int Ed. 2012;51(41):10307–10310. doi: 10.1002/anie.201204475

[26] Hynek J, Ondrušová S, Bůžek DP, et al. Postsynthetic modification of a zirconium metal–organic framework at the inorganic secondary building unit with diphenylphosphinic acid for increased photosensitizing properties and stability. Chem Commun. 2017;53(61):8557–8560. doi: 10.1039/C7CC05068B

[27] Hynek J, Rathouský J, Demel J, et al. Design of porphyrin-based conjugated microporous polymers with enhanced singlet oxygen productivity. RSC Adv. 2016;6(50):44279–44287. doi: 10.1039/C6RA04066G

[28] Zhang Y, Zhang L, Wang Z, et al. Renal-clearable ultrasmall covalent organic framework nanodots as photodynamic agents for effective cancer therapy. Biomaterials. 2019;223:119462. doi: 10.1016/j.biomaterials.2019.119462

[29] Hynek J, Zelenka J, Rathouský J, et al. Designing porphyrinic covalent organic frameworks for the photodynamic inactivation of bacteria. ACS Appl Mater Interfaces. 2018;10(10):8527–8535. doi: 10.1021/acsami.7b19835

[30] Atilgan A, Cetin MM, Yu J, et al. Post-synthetically elaborated BODIPY-based porous organic polymers (POPs) for the photochemical detoxification of a sulfur mustard simulant. J Am Chem Soc. 2020;142(43):18554–18564. doi: 10.1021/jacs.0c07784

[31] Liu Y, Howarth AJ, Hupp JT, et al. Selective photo-oxidation of a mustard-gas simulant catalyzed by a porphyrinic metal–organic framework. Angew Chem Int Ed. 2015;54(31):9001–9005. doi: 10.1002/anie.201503741

[32] Yaghi OM, Li H. Hydrothermal synthesis of a metal-organic framework containing large rectangular channels. J Am Chem Soc. 1995;117(41):10401–10402. doi: 10.1021/ja00146a033

[33] Côté AP, Benin AI, Ockwig NW, et al. Chemistry: porous, crystalline, covalent organic frameworks. Science. 2005;310(5751):1166–1170. doi: 10.1126/science.1120411

[34] Ding SY, Gao J, Wang Q, et al. Construction of covalent organic framework for catalysis: pd/COF-LZU1 in Suzuki–Miyaura coupling reaction. J Am Chem Soc. 2011;133(49):19816–19822. doi: 10.1021/ja206846p

[35] Tilford RW, Gemmill WR, zur Loye HC, et al. Facile synthesis of a highly crystalline, covalently linked porous boronate network. Chem Mater. 2006;18(22):5296–5301. doi: 10.1021/cm061177g

[36] Tilford RW, Mugavero SJ, Pellechia PJ, et al. Tailoring microporosity in covalent organic frameworks. Adv Mater. 2008;20(14):2741–2746. doi: 10.1002/adma.200800030

[37] Kuhn P, Antonietti M, Thomas A. Porous, covalent Triazine-based frameworks prepared by ionothermal synthesis. Angew Chem Int Ed. 2008;47(18):3450–3453. doi: 10.1002/anie.200705710

[38] Farha OK, Spokoyny AM, Hauser BG, et al. Synthesis, properties, and gas separation studies of a robust diimide-based microporous organic polymer. Chem Mater. 2009;21(14):3033–3035. doi: 10.1021/cm901280w

[39] Germain J, Fréchet JMJ, Svec F. Nanoporous polymers for hydrogen storage. Small. 2009;5(10):1098–1111. doi: 10.1002/smll.200801762

[40] Kaur P, Hupp JT, Nguyen ST. Porous organic polymers in catalysis: opportunities and challenges. ACS Catal. 2011;1(7):819–835. doi: 10.1021/cs200131g

[41] Na CJ, Yoo MJ, Tsang DCW, et al. High-performance materials for effective sorptive removal of formaldehyde in air. J Hazard Mater. 2019;366:452–465. doi: 10.1016/j.jhazmat.2018.12.011

[42] Hu YS, Sun YN, Feng ZW, et al. Design and construction strategies to improve covalent organic frameworks photocatalyst's performance for degradation of organic pollutants. Chemosphere. 2022;286:131646. doi: 10.1016/j.chemosphere.2021.131646

[43] Chen D, Liu C, Tang J, et al. Fluorescent porous organic polymers. Polym Chem. 2019;10(10):1168–1181. doi: 10.1039/C8PY01620H

[44] Milgrom LR. The facile aerial oxidation of a porphyrin. Tetrahedron. 1983;39(23):3895–3898. doi: 10.1016/S0040-4020(01)90892-0

[45] Kim DS, Sessler JS. Calix[4]pyrroles: versatile molecular containers with ion transport, recognition, and molecular switching functions. Chem Soc Rev. 2014;44(2):532–546. doi: 10.1039/C4C500157E

[46] Hill JP, Schumacher AL, D'Souza F, et al. Chromogenic indicator for anion reporting based on an N-substituted oxoporphyrinogen. Inorg Chem. 2006;45(20):8288–8296. doi: 10.1021/ic0611591

[47] Hill JP, Hewitt IJ, Anson CE, et al. Highly nonplanar, electron deficient, N-substituted tetra-oxocyclohexa-dienylidene porphyrinogens: structural, computational, and electrochemical investigations. J Org Chem. 2004;69(18):5861–5869. doi: 10.1021/jo049401d

[48] Shundo A, Labuta J, Hill JP, et al. Nuclear magnetic resonance signaling of molecular chiral information using an achiral reagent. J Am Chem Soc. 2009;131:9494–9495. doi: 10.1021/ja903371d

[49] Chahal MK, Payne DT, Labuta J, et al. Selective phase transfer reagents (OxP-crowns) for chromogenic detection of nitrates especially ammonium nitrate. Chem: Eur J. 2020;26(58):13177–13183. doi: 10.1002/chem.202003166

[50] Chahal MK, Payne DT, Matsushita Y, et al. Molecular engineering of β-substituted oxoporphyrinogens for hydrogen-bond donor catalysis. Eur J Org Chem. 2020;2020(1):82–90. doi: 10.1002/ejoc.201901706

[51] D'Souza F, Subbaiyan NK, Xie Y, et al. Anion-complexation-induced stabilization of charge separation. J Am Chem Soc. 2009;131(44):16138–16146. doi: 10.1021/ja9048306

[52] Hynek J, Payne DT, Chahal MK, et al. Enhancement of singlet oxygen generation based on incorporation of oxoporphyrinogen (OxP) into microporous solids. Mater Today Chem. 2021;21:100534. doi: 10.1016/j.mtchem.2021.100534

[53] Golder AJ, Milgrom LR, Nolan KB, et al. 5,10,15,20-Mesotetrakis(3,5-di-t-butyl-4-quinoemethide)porphyrinogen: a highly puckered tetrapyrrolic macrocycle from the facile aerial oxidation of a phenolic porphyrin. J Chem Soc, Chem Commun. 1989;(22):1751–1753. doi: 10.1039/C39890001751

[54] Milgrom LR, Hill JP, Yahioglu G. Facile aerial oxidation of a porphyrin. Part 18. N-alkylation of the oxidised product derived from meso-tetrakis(3,5-di-t-butyl-4-hydroxyphenyl)porphyrin. J Heterocycl Chem. 1995;32(1):97–101. doi: 10.1002/jhet.5570320117

[55] Fang Q, Wang J, Gu S, et al. 3D porous crystalline polyimide covalent organic frameworks for drug delivery. J Am Chem Soc. 2015;137(26):8352–8355. doi: 10.1021/jacs.5b04147

[56] Chlebosz D, Goldeman W, Janus K, et al. Synthesis, solution, and solid state properties of homological dialkylated naphthalene diimides—A systematic review of molecules for next-generation organic electronics. Molecules. 2023;28(7):2940. doi: 10.3390/molecules28072940

[57] Li Q, Hou W, Peng F, et al. Photothermal conversion performance of perylene diimide radical anion salts modified with tunable moieties. J Mater Sci. 2019;54(1):217–227. doi: 10.1007/s10853-018-2822-2

[58] Fajal S, Dutta S, Ghosh SK. Porous organic polymers (POPs) for environmental remediation. Mater Horiz. 2023;10(10):4083–4138. doi: 10.1039/D3MH00672G

[59] Hynek J, Chahal MK, Payne DT, et al. Design rules for oxoporphyrinogen ('OxP') as a versatile chromophore for efficient singlet oxygen generation. J Porphyrins Phthalocyanines. 2023;27(7n10):1108–1118. doi: 10.1142/S1088424623500359

[60] Milgrom LR, Hill JP. Aerial oxidation kinetics of a phenolic porphyrin in acid solution. J Heterocycl

Chem. 1993;30(6):1629–1633. doi: 10.1002/jhet. 5570300628

[61] Milgrom LR, Hill JP, Flitter WD. Formation of hydroxyl radicals during the facile aerial oxidation of a phenolic porphyrin. J Chem Soc, Chem Commun. 1992;1992(10):773–775. doi: 10.1039/C39920000773

[62] Březina V, Ishihara S, Lang J, et al. Structural modulation of chromic response: effects of binding-site blocking in a conjugated calix[4]pyrrole chromophore. ChemistryOpen. 2018;7(5):323–335. doi: 10.1002/open.201800005

[63] Tsoutsoupoulos A, Brockmöller S, Thiermann H, et al. Comparison of the toxicity of sulfur mustard and its oxidation products in vitro. Toxicol Lett. 2020;321:69–72. doi: 10.1016/j.toxlet.2019.12.015

[64] Liang J-J, Gu C-L, Kacher ML, et al. Chemistry of singlet oxygen. 45. Mechanism of the photooxidation of sulfides. J Am Chem Soc. 1983;105(14):4717–4721. doi: 10.1021/ja00352a033

[65] Doherty S, Knight JG, Carroll MA, et al. Efficient and selective hydrogen peroxide-mediated oxidation of sulfides in batch and continuous flow using a peroxometalate-based polymer immobilized ionic liquid phase catalyst. Green Chem. 2015;17:1559–1571. doi: 10.1039/C4GC01770F

[66] Mba M, Prins HJ, Licini G. C_3-symmetric Ti(IV) triphenolate amino complexes as sulfoxidation catalysts with aqueous hydrogen peroxide. Org Lett. 2007;9(1):21–24. doi: 10.1021/ol062395i

[67] Schöneich C, Aced A, Asmus K-D. Mechanism of oxidation of aliphatic thioethers to sulfoxides by hydroxyl radicals. The importance of molecular oxygen. J Am Chem Soc. 1993;115(24):11376–11383. doi: 10.1021/ja00077a042

[68] Bosio GN, Parisi J, Einschlag FSG, et al. Imidazole and beta-carotene photoprotection against photodynamic therapy evaluated by synchrotron infrared microscopy. Spectrochimica Acta A Mol Biomol Spectroscopy. 2018;195:53–61. doi: 10.1016/j.saa. 2018.01.027

[69] Zhang R, Song X, Liu Y, et al. Monomolecular VB_2-doped MOFs for photocatalytic oxidation with enhanced stability, recyclability and selectivity. J Mater Chem A. 2019;7(47):26934–26943. doi: 10.1039/C9TA09571C

[70] Wei H, Guo Z, Liang X, et al. Selective photooxidation of amines and sulfides triggered by a superoxide radical using a novel visible-light-responsive metal–organic framework. ACS Appl Mater Interfaces. 2019;11(3):3016–3023. doi: 10.1021/acsami.8b18206

[71] Feng X, Wang X, Wang H, et al. Elucidating J-aggregation effect in boosting singlet-oxygen evolution using zirconium–porphyrin frameworks: a comprehensive structural, catalytic, and spectroscopic study. ACS Appl Mater Interfaces. 2019;11(48):45118–45125. doi: 10.1021/acsami. 9b17569

[72] Lu G, Chu F, Huang X, et al. Recent advances in metal-organic frameworks-based materials for photocatalytic selective oxidation. Coord Chem Rev. 2022;450:214240. doi: 10.1016/j.ccr.2021. 214240